International Journal of Engineering Science 220 (2026) 104436

Contents lists available at ScienceDirect

International Journal of Engineering Science

journal homepage: www.elsevier.com/locate/ijengsci

Full length article

Impact-governed dynamics of an axially-incompressible bistable continuous metastructure

Andrea Nobili [a,b,*], Dipendu Pramanik [a]

[a] Department of Engineering Enzo Ferrari, University of Modena and Reggio Emilia, via Vivarelli 10, 41125 Modena, Italy
[b] National Group for Mathematical Physics (GNFM), Institute for Higher Mathematics Francesco Severi (INdAM), Piazzale Aldo Moro, 5, 00185 Rome, Italy

ARTICLE INFO

Keywords:
Impacts
Incompressible string
Variational equality
Complementarity

ABSTRACT

We study the dynamics of a bistable Single Degree of Freedom mechanism that bifurcates from the trivial straight configuration when subjected to a critical traction force and it is otherwise incompressible. We show that the appearance of "impacts", in correspondence with the minimum axial extension of the system, merely reflects the adoption of the axial extension as the dependent variable, as opposed to the angular rotation. Within this description, the structure realizes a perfectly elastic obstacle. Next, we construct the continuous limit for a dense chain of such mechanisms and axial strain naturally emerges as the continuous dependent field. Consequently, an unilateral constraint becomes associated with the system. Most importantly, the corresponding Lagrangian problem needs to be supplemented by energy conservation across the impacts to faithfully represent the underlying microstructure. In doing so, we generalize the established procedure to construct the continuous limit of a dense chain of discrete systems to the presence of unilateral constraints. Remarkably, energy conservation allows to apply Hamilton's principle in the form of a variational *equality*, in contrast to the inequality format usually encountered when dealing with non-smooth problems. This important result, which greatly simplifies the mathematics, is available provided that variations are extended to accommodate for discontinuities in the variables. Besides, the system dynamics may be now constructed semi-analytically by joining pairs of d'Alembert's solutions through the conditions obtained from the extended variational principle at the impact time and location (which are obviously unknown). As a result, waves propagating in the system are obtained and they are checked against global energy conservation.

1. Introduction

Mechanical metastructures are engineered systems purposefully designed to exhibit unconventional mechanical properties that arise not just from the material response, but mostly from the carefully devised geometrical architecture. A particularly intriguing aspect of these systems is their ability to harness instabilities, traditionally associated with failure, as functional mechanisms to achieve special purposes, for example tunability, deployability and locomotion. Indeed, in classical mechanics, instabilities such as buckling, snapping, or folding, often forgo loss of structural integrity. In contrast, in mechanical metastructures, these instabilities can be deliberately introduced and even precisely controlled to enable a wide range of novel behaviours among which we mention programmable stiffness (Mukhopadhyay et al., 2020), shape morphing (Hutchinson, 1974; Overvelde et al., 2012), negative stiffness

* Corresponding author at: Department of Engineering Enzo Ferrari, University of Modena and Reggio Emilia, via Vivarelli 10, 41125 Modena, Italy.
E-mail address: andrea.nobili@unimore.it (A. Nobili).

https://doi.org/10.1016/j.ijengsci.2025.104436
Received 26 August 2025; Received in revised form 27 November 2025; Accepted 29 November 2025
Available online 7 December 2025

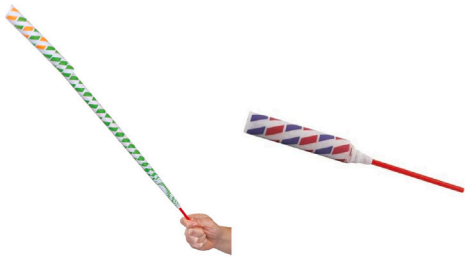

Fig. 1. A paper flicker toy is composed of many paper rings which may be extended telescopically (left) far beyond their (minimum) original length (right).

responses (Lee & Goverdovskiy, 2012), and energy absorption (Yap et al., 2008). By embedding instabilities into their design, engineers can create structures that transition between multiple stable or metastable states, paving the way for applications in soft robotics, deployable architectures, locomotion and mechanical logic. For example, overhanging elements in cellular lattices can buckle under compression to produce large, reversible deformations that serve as mechanical switches or actuators (Florijn et al., 2014; Shan et al., 2015).

The recognition of mechanical instabilities as key design factors can be traced back to the early studies on buckling in slender structures, such as Euler's buckling of beams. However, it was not until the last two decades that researchers began systematically integrating instabilities into engineered architectures for performance *enhancement*. Notably, over the past decade, buckling has been reframed as a controllable, reversible, and often beneficial phenomenon (Coulais et al., 2016; Gladman et al., 2016; Rafsanjani et al., 2019). Snap-through instabilities in bistable elements, such as curved beams or kirigami-based patterns, enable rapid transitions between configurations, useful in deployable systems and soft robotics (Rafsanjani & Bertoldi, 2017; Waitukaitis et al., 2015). Wrinkling, folding, and creasing instabilities have also found utility in thin-film and shell-based metastructures. These deformation modes can be finely tuned by geometric and material parameters, enabling reconfigurable surfaces and responsive skins (Holmes et al., 2010; Pocivavsek et al., 2008; Volpini et al., 2022).

Despite the large body of literature available on the subject, it appears that no consideration has yet been given to the existence of finite intervals of admissibility for the deformation, which are often due to geometrical constraints. This is all the more surprising given the recognition of *large deformations* as the key driver for disclosing the full potential of metastructures. The fact that deformations are often geometrically bounded introduces unilateral constraints in the system and therefore greatly complicates the analysis. Specifically, the classical variational equality associated with Hamilton's principle is now replaced by a *variational inequality*, whose application requires concepts of convex and non-smooth analysis, see the monographs by Brogliato (1999) and Kravchuk and Neittaanmäki (2007). The mathematical machinery required to address the problem was first introduced by Ostrogradski in connection with discrete mechanics (Kozlov & Treshchëv, 1991), and then later extended by Signorini to continuum mechanics, in what is now known as *Signorini's problem* (Kravchuk & Neittaanmäki, 2007).

As a noticeable exception, very recently Hima et al. (2023), while extending to dynamics their work on metainterfaces (Hima et al., 2022), observed the presence of an unilateral constraint realized by an incompressible member in the structure. As a consequence of this, "various impact scenarios", named "bouncing, no-bouncing or partial-bouncing", were acknowledged and "strong similarities with the rocking motions of rigid blocks" found. This observation is the starting point of this paper, that specifically investigates how these "impacts" may emerge from a smooth and energy-conserving mechanism (the presence of dissipation is immaterial to our present argument). Indeed, Section 2 studies the dynamics of a traction unstable mechanism (see Fig. 2), that was introduced by Zaccaria et al. (2011) as an example of traction-induced instability, which realizes the incompressibility constraint. The dynamics of the system is solved in closed form in Section 3 and reveals strong similarities with that of a pendulum. In fact, it is shown that the appearance of "impacts" is merely due to the choice of the axial strain as the dependent variable and it would be absent otherwise. Therefore, one and only one impact scenario is possible, which accounts for energy conservation and a unitary restitution coefficient. This consideration is exploited in Section 4, where the continuous limit of a dense chain of mechanisms is developed by adopting the axial strain as the dependent continuous variable. The resulting system behaves similarly to a flicker toy, Fig. 1, which may be elastically extended beyond its minimum packed length. To correctly account for the way axial incompressibility is realized, *energy conservation across the impacts must be embedded in the formulation*. Specifically, Section 4.1 develops the correct Hamiltonian formulation and, in doing so, it extends the classical procedure which is adopted to develop the continuous limit of a discrete chain, see for example Rosenau (2003). Surprisingly, Hamilton's principle holds in the form of a variational *equality*, provided that account is made of possible jumps in the dependent variables. This result has far reaching consequences for it gets away from the complex machinery of non-smooth mechanics. The extended version of Hamilton's principle is developed in Appendix and applied in Section 4.3 to join pairs of D'Alembert solutions through the unknown impact locations, which are numerically defined in both time and space. Finally, conclusions are drawn in Section 5.

2. A traction unstable incompressible mechanism

Let us consider the Single Degree of Freedom (SDOF) system, illustrated in Fig. 2, composed by a pair of rigid rods, each of length ℓ: The left rod is connected to a hinge and the right rod to a roller and they are joined together through an elastic slider,

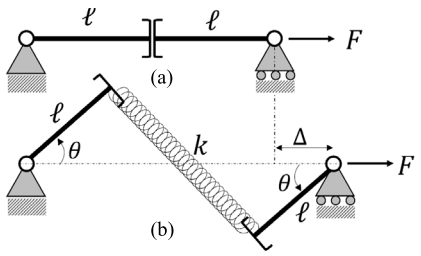

Fig. 2. Traction unstable mechanism realized with two rigid bars connected together by an elastic slider: the system is indefinitely extensible by the amount Δ beyond the minimum length 2ℓ, i.e. $\Delta \geq 0$.

see Palumbo et al. (2018), Zaccaria et al. (2011). This last constraint allows for transversal (to the rods' axis) movements, to which it opposes an elastic reaction, while it preserves parallelism between the rods, as in Fig. 2(b). The system is described by the angle $\theta \in (-\pi/2, \pi/2)$, which measures the rotation of each rod with respect to the undeformed configuration wherein the rods are aligned along the x-axis. For such system, upon any rotation θ, the elongation $\Delta = 2\ell(\sec\theta - 1)$ is produced and the corresponding strain follows

$$\varepsilon = \sec\theta - 1. \tag{1}$$

Within the admissible range of θ, it holds the constraint for the strain

$$\varepsilon \geq 0. \tag{2}$$

The potential energy of the system reads

$$V = \tfrac{1}{2}k(2\ell\tan\theta)^2 - F\Delta, \tag{3}$$

where F is the longitudinal force applied to the roller and $k > 0$ is the stiffness of the spring connecting the rods across the slider. Similarly to the configuration studied in Zaccaria et al. (2011), this system possesses a point symmetry $\theta \leftrightarrow -\theta$, whereupon we will restrict the analysis to positive θ, with the understanding that negative values are equally possible. It is easily seen that two static equilibrium configurations (branches) are admitted, namely the trivial solution $\theta \equiv 0$ as well as the bifurcated solution

$$\theta_s = \arccos\eta^{-1}, \quad \eta = \frac{F}{F_{cr}}, \tag{4}$$

where $F_{cr} = 2k\ell$ is the critical load. Clearly, this is a continuous bifurcation and analysis of the second derivative shows that the trivial solution proves stable inasmuch as $F < F_{cr}$, i.e. $\eta < 1$, and then the bifurcated solution takes over. It should be emphasized that the trivial equilibrium solution sits right at the boundary of the admissible domain (2), whence it deserves special consideration.

Let us introduce the kinetic energy

$$K = \tfrac{1}{2}m\dot{\Delta}^2, \tag{5}$$

having assumed, for simplicity and to avoid rotational inertia, that the mass m of the system is located at the end connected to the roller. Here, a superposed dot is shorthand for time differentiation, i.e. $\dot{\Delta} = \mathrm{d}\Delta/\mathrm{d}t$. The Lagrangian function reads

$$L = K - V = 2k\ell^2\frac{\sin^2\theta}{\cos\theta}\left(2\eta\frac{1}{\cos\theta+1} + \frac{\sec^3\theta}{\omega^2}\dot{\theta}^2 - \sec\theta\right), \tag{6}$$

where, as in standard practice, we have let the frequency $\omega = \sqrt{k/m} > 0$. The Euler–Lagrange equation is easily derived

$$F_{cr}\Theta f(\theta, \dot{\theta}, \ddot{\theta}) = 0, \tag{7}$$

where

$$f(\theta, \dot{\theta}, \ddot{\theta}) = \omega^{-2}\left[\dot{\theta}^2\frac{\sin^2\theta + 1}{\cos^3\theta} + \ddot{\theta}\frac{\sin\theta}{\cos^2\theta}\right] - \eta + \sec\theta, \tag{8}$$

and

$$\Theta = \frac{\mathrm{d}\Delta}{\mathrm{d}\theta} = 2\ell\frac{\sin\theta}{\cos^2\theta}. \tag{9}$$

Clearly, Eq. (7) is satisfied when either $\Theta = 0$ (i.e. Δ is constant w.r.t. θ), which amounts to the trivial solution $\theta = 0$, or when $f(\theta, 0, 0) = 0$, which lends the bifurcated solution (4).

2.1. Linearized system

We now perform a linear phase space analysis of this 1 DOF system to highlight the main features of its dynamics. The set of admissible motions depends on whether the applied force F sits below (sub-critical) or above (super-critical) the threshold force F_{cr}, which triggers the bifurcation.

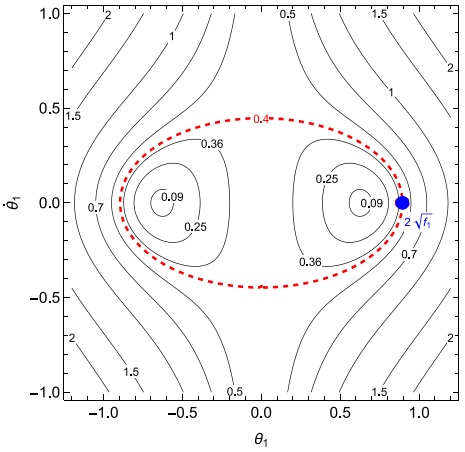

Fig. 3. Phase space diagram of the first integral (16) for $\omega = 1$, $f_1 = 0.2$. Labels provide the energy levels h_1, while the blue dot indicates the maximum angle $\theta_{sep} = 2\sqrt{f_1}$ reached by the separatrix (red, dashed curve).

2.1.1. Supercritical load

The nonlinear second order autonomous ODE (8) may be linearized asymptotically in the vicinity of and beyond the critical load F_{cr} through letting $\theta = \epsilon\theta_1$, i.e. for $\eta = 1 + \epsilon^2 f_1$, $f_1 \geq 0$. To leading order, one finds the nonlinear ODE

$$\ddot{\theta_1} = -\tfrac{1}{2}\omega^2\theta_1 - \frac{(\dot{\theta_1})^2}{\theta_1} + f_1\frac{\omega^2}{\theta_1}, \quad \theta_1 \neq 0. \tag{10}$$

One obvious solution of this equation is the bifurcated static solution (4), where F is expanded about F_{cr}, namely

$$\theta_1(t) \equiv \theta_{1s} = \sqrt{2f_1}, \quad f_1 \geq 0. \tag{11}$$

Indeed, as expected, Eq. (10) simply reduces to the pendulum equation provided that we operate the variable change

$$\beta(t) = \theta_1^2(t) - \theta_{1s}^2, \tag{12}$$

that is proportional to the angular distance from the bifurcated solution. Thus, Eq. (10) lends

$$\ddot{\beta} = -\omega^2\beta,$$

with the classical first integral

$$\dot{\beta}^2 = h_1^2 - \omega^2\beta^2, \tag{13}$$

where, as we shall see in the following, $h_1 \geq 0$ is an integration constant related to the energy of the system. As well known, this first integral can be integrated by quadrature to lend the simple harmonic motion (SHM)

$$\beta(t) = A\cos\left[\omega(t - t_0)\right], \tag{14}$$

where $A = h_1\omega^{-1}$ is an amplitude and t_0 any reference time. According to Eqs. (12) and (13), for the velocity $\dot{\beta}$ to be real it needs to be

$$A > |\beta| = |\theta_1^2 - 2f_1|. \tag{15}$$

In the original variable θ_1, the first integral (13) reads

$$\dot{\theta_1} = \pm\frac{h_1}{2\theta_1}\sqrt{1 - A^{-2}\left(\theta_1^2 - \theta_{1s}^2\right)^2}. \tag{16}$$

which allows for a classical phase space analysis. From (16) it is clear that the inequality (15) simply demands that the square root lends real values. The first integral (16) is plotted in Fig. 3 for $\omega = 1$ and $f_1 = 0.2$. Two stable equilibrium points (centers) are clearly identified corresponding to the bifurcated solutions (11). The neighbouring phase paths are closed curves, which occur in the range $0 < \theta_1 \leq \theta_M$, where

$$\theta_M = \sqrt{2f_1 + A}, \tag{17}$$

up to a threshold value for the energy $h = h_{sep}$, upon reaching which the phase path goes through the trivial solution $\theta_1 = 0$ with velocity $\dot{\theta}_1 = \omega\sqrt{f_1}$. This limiting phase path is the *separatrix* between periodic and whirling motions. The equation of the separatrix is obtained demanding that the RHS of (16) is meaningful (bounded) as $\theta_1(t) \to 0$, which condition lends

$$A = 2f_1, \quad \Leftrightarrow \quad h_{sep} = 2\omega f_1, \tag{18}$$

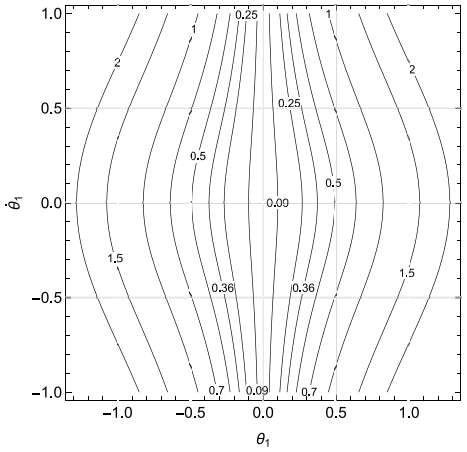

Fig. 4. Phase space analysis of the first integral (16) for $\omega = 1$, $f_1 = -0.2$ at different energy levels h_1: only the whirling motion occurs about the trivial solution $\theta_1 = 0$.

and, in the case of Fig. 3, it is $h_{sep} = 0.4$. The separatrix lies in the strip $|\theta_1| \le \theta_{sep} = 2\sqrt{f_1}$. It is thus seen that, within this linear analysis, the separatrix is the only phase path that goes through the trivial solution and for which impact with the constraint is possible.

For energy levels beyond the separatrix, $h > h_{sep}$, it is $|\theta_1| \le \theta_M$ where the maximum angle is reached with the classical period of the linear harmonic oscillator, which is isochronous,

$$T = Ah_1^{-1} \int_{-1}^{1} \frac{\mathrm{d}u}{\sqrt{1-u^2}} = \frac{\pi}{\omega}. \tag{19}$$

To see this, we can rewrite (16) through the variable $u = (\theta_1^2 - 2f_1)/A$ for which $|u| \le 1$, and realize that phase paths are closed at infinity letting $\dot{\theta}_1$ flip its sign as $\theta_1 \to 0$. In this context, the bifurcated solution is never stable and the trivial solution $\theta_1 = 0$ is reached with infinite velocity. Indeed, expanding (16) in the vicinity of the separatrix, that is for $h_1 = h_{sep} + h_2$, and for $\theta \ll 1$, one finds

$$\dot{\theta} = \sqrt{\omega f_1}\frac{\sqrt{h_2}}{\theta} + O(\theta/\sqrt{h_2}), \tag{20}$$

which shows that the rotational speed diverges as θ^{-1} within the distinct limit $\theta \ll \sqrt{h_2}$. To better appreciate this point we observe that

$$\varepsilon = \tfrac{1}{2}\theta^2 + O(\theta^4), \quad \text{whence} \quad \dot{\varepsilon} = \theta\dot{\theta} + O(\epsilon^4), \tag{21}$$

and consequently the rotational speed tends to infinity whereas the longitudinal rate of deformation $\dot{\varepsilon}$ tends to a constant.

2.1.2. Subcritical load

It is important to point out that the variable change (12) is meaningful inasmuch as $\beta + 2f_1 \ge 0$. For $f_1 < 0$, the axial force in the system is not quite large enough to guarantee the stability of the bifurcated solution, i.e. we are sitting below the critical point. We can explore the situation $f_1 < 0$ by looking for solutions in the neighbourhood of the trivial solution through the variable change

$$\beta(t) = \theta_1^2(t), \tag{22}$$

whence we get

$$\ddot{\beta} = 2\omega^2 f_1 - \omega^2\beta, \tag{23}$$

with the first integral

$$\dot{\beta}^2 = h_1^2 + 4\omega^2 f_1\beta - \omega^2\beta^2, \tag{24}$$

that reads, in the original variable,

$$\dot{\theta}_1 = \pm\frac{h_1}{2\theta_1}\sqrt{1 + A^{-2}\theta_1^2(4f_1 - \theta_1^2)}, \quad f_1 \le 0, \tag{25}$$

which coincides with (16) upon letting $f_1 = 0$. The phase diagram for $f_1 < 0$ is shown in Fig. 4 for different energy levels and it is seen that only whirling motions about the trivial solution are admitted. Clearly, the trivial solution is now generally unstable. All such results will be confirmed by the phase space analysis of the nonlinear system in Section 2.2.

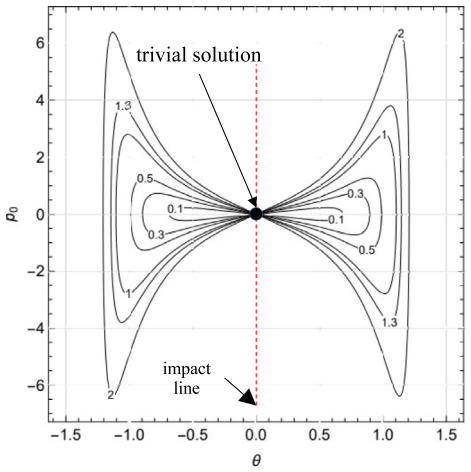

Fig. 5. Canonical butterfly-shaped phase diagram for $\eta = 0.8$ (below the critical threshold) at different values of the system energy h_0: phase paths are all composed by homoclinic orbits going through the trivial solution (the origin).

2.2. Hamiltonian of the discrete system

We now write the dimensionless Hamiltonian density $H_0 = (2\ell F_{cr})^{-1} H$ of this SDOF system

$$H_0 = \tfrac{1}{2} {p_0}^2 \frac{\cos^4\theta}{\sin^2\theta} - (\eta - 1 - \tfrac{1}{2}\varepsilon)\varepsilon, \tag{26}$$

where we have let the *dimensionless* conjugate momentum

$$p_0 \equiv \frac{p}{4l^2\, m\omega} = \omega^{-1} \tan^2\theta \sec^2\theta\, \dot\theta, \tag{27}$$

and ε is the strain (1). To draw a connection with the linear analysis of the previous Section, we expand the momentum (27) and the Hamiltonian (26) with respect to $\theta \ll 1$ and in the vicinity of the critical load, to get

$$H_0 = \tfrac{1}{2}\omega^{-2}\theta^2\dot\theta^2 - \tfrac{1}{8}\theta^2\left(4f_1 - \theta^2\right) + o(\theta^2), \tag{28}$$

and looking for the solution curves $H_0 = h_1^2/(8\omega^2)$ we retrieve the first integral (25).

The canonical system of equations lends back (27) in the form

$$\dot\theta = \omega \frac{\partial H_0}{\partial p_0} = \omega \cos^2\theta \cot^2\theta\, p_0,$$

which may be rewritten in terms of strain and strain rate

$$p_0 = \omega^{-1} \operatorname{sgn}\theta(\epsilon + 1)\sqrt{\epsilon(\epsilon+2)}\dot\epsilon, \tag{29}$$

where $\operatorname{sgn}\theta$ is the signum function. In the same manner, we get the second canonical equation

$$\dot p_0 = -\omega \frac{\partial H_0}{\partial \theta} = \omega \frac{\sin\theta}{\cos^2\theta}(\eta - \sec\theta) + {p_0}^2 \omega \cot^3\theta\left(1 + \sin^2\theta\right), \tag{30}$$

and indeed, together, Eqs. (27) and (30) amount to the Euler–Lagrange equation (7).

2.2.1. Subcritical load

As well known, the Hamiltonian (26) provides a first integral for the motion and allows us to develop a phase plane analysis considering the level curves $H_0 = h_0$. For $\eta < 1$, that is below the critical force F_{cr}, the butterfly-shaped phase paths are plotted in Fig. 5, which shows that only homoclinic orbits are encountered, all of which go through the trivial solution $(\theta, p_0) = (0, 0)$. This result is reconciled with the linearized result depicted in Fig. 4, which highlighted whirling motions in the $(\theta, \dot\theta)$ plane, by noting that

$$p_0 = \omega^{-1}\theta^2\dot\theta + O(\theta^3), \quad \text{as} \quad \theta \to 0, \tag{31}$$

which means that, although $\dot\theta$ diverges as $O(\theta^{-1})$ per Eq. (20), the dimensionless momentum tends to zero.

This behaviour may be investigated further by looking at the Hamiltonian (34) rewritten in terms of strain ε and strain rate $\dot\varepsilon$ as

$$H_0 = \tfrac{1}{2}\omega^{-2}\dot\varepsilon^2 + \tfrac{1}{2}\varepsilon\left[\varepsilon + 2(1-\eta)\right], \tag{32}$$

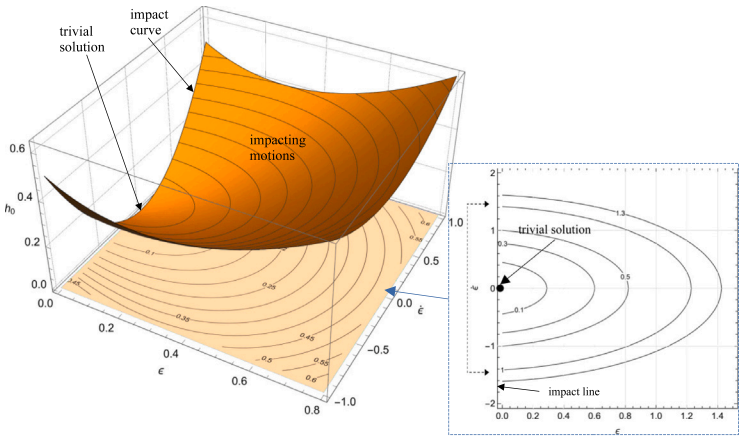

Fig. 6. System energy (left) for $\eta = 0.8$ and $\omega = 1$ in terms of strain ε and strain rate $\dot{\varepsilon}$: Phase paths corresponding to different energy levels are projected onto the plane $h_0 = 0$ which marks the transition to periodic oscillations around the bifurcated solution. For any given energy level h_0, phase paths start and end onto the unilateral constraint $\varepsilon \geq 0$ (right), yet they should be closed by flipping the sign of the strain rate $\dot{\varepsilon}$ (dashed line).

that is plotted in Fig. 6, accounting for the constraint $\varepsilon \geq 0$. The corresponding phase diagram (right plot in Fig. 6) seems to indicate that an "impact" occurs upon reaching $\varepsilon = 0$ with dimensionless kinetic energy $\frac{1}{2}\omega^{-2}\dot{\varepsilon}^2 = h_0 > 0$. However, this misinterpretation is immediately dispelled accounting for energy conservation through the continuous variable θ, which warrants that each phase curve that hits $\varepsilon = 0$ with speed $\pm\dot{\varepsilon}$ should be continued with speed $\mp\dot{\varepsilon}$ respectively. The same conclusion may be reached by looking at the momentum definition (29). If we agree to call *impact* any jump in the momenta, we see that Eq. (29) suggests that a momentum jump occurs every time θ changes sign, i.e. goes through zero, *provided that* $\sqrt{\varepsilon} \neq 0$. However, as it was already observed, the position $\theta = 0$ occurs alongside zero elongation $\varepsilon = 0$, from which it is deduced that no momentum jump can take place. Yet, letting the *longitudinal momentum* of the roller, wherein all mass is concentrated as in a point mass,

$$\mu = m\dot{\Delta} = 2\ell m\dot{\epsilon}, \tag{33}$$

it is seen that the conjugate momentum is the product $p = \Theta\mu$, where Θ is defined in (9). Then, it appears that the jump in the longitudinal momentum μ taking place at $\theta = 0$, as demonstrated in Fig. 6, occurs alongside $\Theta = 0$, whence p remains continuous (in fact, zero). We conclude that, when looking in the plane $(\epsilon, \dot{\epsilon})$, one may be led to believe that an impact occurs where, in fact, it is the choice of the variables which indulges in such misinterpretation. This important observation stands on the fact that the kinetic energy (5) of the system is associated with the rotation of the rigid rods through the angle θ which, however, does not carry inertia in itself but through the longitudinal motion. Accordingly, for the energy to be preserved through $\theta = 0$, wherein the elongation disappears, an infinite rotational velocity is demanded so that the elongation rate is finite and indeed accounts, through the kinetic energy, for the whole energy of the system. When the microstructural angle θ is used as the coordinate of the system, the problem has no constraint attached, for θ may vary in continuous fashion (in the given domain). Conversely, when the problem is entirely described in terms of the strain ε, it becomes subjected to the unilateral constraint $\varepsilon \geq 0$, and yet account should be made of the fact that the underlying microstructure preserves the kinetic energy of the system upon hitting the constraint. Within this viewpoint, it appears that the microstructure, therefore, realizes a perfectly elastic impact.

2.2.2. *Supercritical load*

We rewrite the Hamiltonian (26) as

$$H_0 = \frac{{p_0}^2}{2\varepsilon(\varepsilon+1)^2(\varepsilon+2)} + \left[\tfrac{1}{2}\varepsilon + 1 - \eta\right]\varepsilon, \tag{34}$$

and observe that this is the sum of two positive terms inasmuch as $\eta < 1$, i.e. we are below the bifurcation threshold. Consequently, the Hamiltonian is a monotonic increasing function of ε and p_0, although it is not quadratic. When $\eta > 1$, the Hamiltonian attains negative values, and specifically two minima appear

$$H_{0min} = -\tfrac{1}{2}(\eta - 1)^2, \tag{35}$$

that are located in correspondence of the bifurcated solutions (see Fig. 8)

$$p_0 = 0, \quad \text{and} \quad \varepsilon = \eta - 1. \tag{36}$$

As anticipated by the linear analysis, it is now possible to have periodic solutions (centers) revolving about such minima, moving alongside periodic orbits, as in Fig. 7 (right), which never reach the trivial solution $\theta = 0$. Conversely, for $h_0 > 0$, periodic solutions

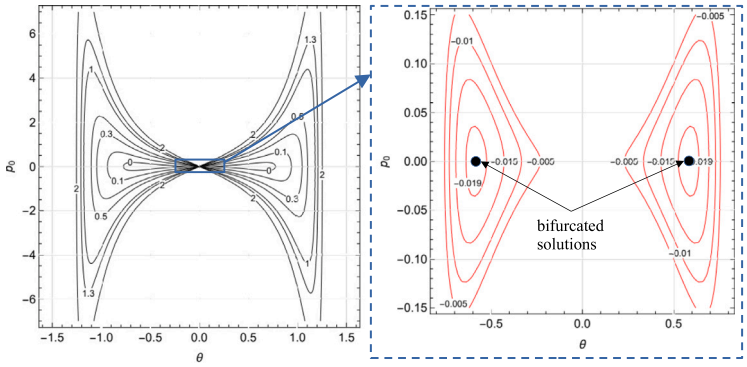

Fig. 7. Canonical phase space diagram for $\eta = 1.2$ and $\omega = 1$ for positive (left) and negative (right) values h_0 of the Hamiltonian. The minimum of the energy (35) corresponds to $h_{min} = -0.02$ and it is located at the bifurcated solution (36).

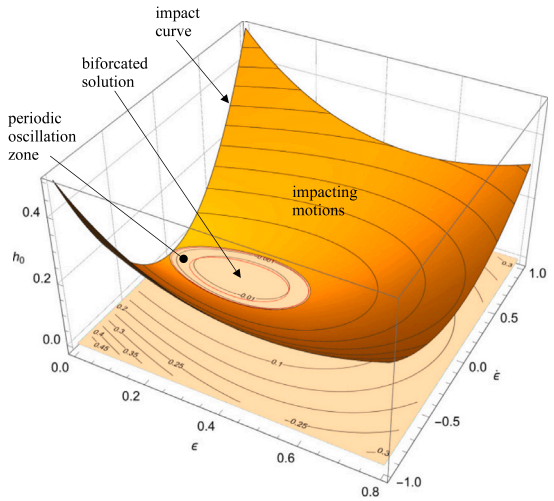

Fig. 8. System energy (hamiltonian) for $\eta = 1.2$ and $\omega = 1$ in terms of strain ϵ and strain rate $\dot{\epsilon}$: Phase paths corresponding to different energy levels h_0 are projected onto the plane $h_0 = 0$ which marks the transition from impacting motions to periodic oscillations around the bifurcated solution.

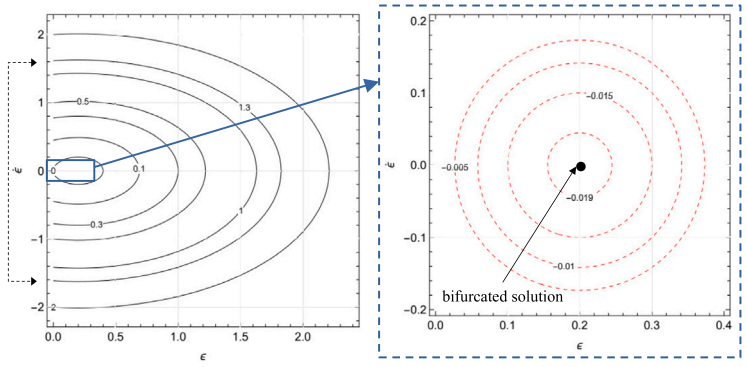

Fig. 9. Phase space diagram in terms of strain rate for $\eta = 1.2$ and $\omega = 1$ for positive (left) and negative (right) values h_0 of the Hamiltonian. Impact occurs at $\epsilon = 0$ but the energy is conserved and trajectories are closed by flipping the sign of the strain rate $\dot{\epsilon}$ (dashed line).

turn into homoclinic orbits which do go through the origin, as in the case of $F < F_{cr}$, see Fig. 7 (left). It is now important to understand how the system behaves when moving across $\theta = 0$ for $\eta > 1$ in the homoclinic trajectories. Fig. 9 shows the phase diagram already depicted in Fig. 7, yet this time in the plane $(\epsilon, \dot{\epsilon})$ and accounting for the constraint $\epsilon \geq 0$. Clearly, periodic solution,

which appear for negative energy values, do not intersect the constraint (loosened states), while, for positive energy levels $h_0 > 0$, trajectories "impact" against the constraint. The effect of this impact may be better investigated moving in the neighbourhood of $\theta \ll 1$, where we see that $\varepsilon \sim \frac{1}{2}\theta^2$ is very small and the first term at RHS of (34) blows up, while the second vanishes. Therefore, we find the trajectories

$$p_0 \approx \pm\sqrt{2\varepsilon h_0} \approx \pm\theta\sqrt{h_0}, \tag{37}$$

corresponding to any $H_0 = \frac{1}{2}h_0 > 0$. Indeed, we have seen that, for $h_0 < 0$, periodic oscillations about the bifurcated equilibrium points take place, which cannot reach $\theta = 0$. By (27), we get, to leading order,

$$p_0 \approx -\omega^{-1}\theta^2\dot{\theta}, \tag{38}$$

whence, putting together (37) and (38), we find the trajectories

$$\varepsilon \sim \tfrac{1}{2}\theta^2 = \sqrt{h_0}\omega|t|, \tag{39}$$

assuming $\theta \to 0$ as $t \to 0$ and where the absolute value was introduced because ε at the LHS is clearly positive. Taking the first and the second time derivatives one gets

$$\dot{\varepsilon} = \sqrt{h_0}\omega\left[2\delta(t)t + 2\,\mathrm{H}(t) - 1\right], \tag{40}$$

and

$$\ddot{\varepsilon} = \sqrt{h_0}\omega\left[2\dot{\delta}(t)t + 4\delta(t)\right], \tag{41}$$

where $\mathrm{H}(t)$ is Heaviside function, whose derivative is Dirac's delta function, i.e. $\delta(t) = \dot{\mathrm{H}}(t)$. Then, either by direct application of (40) or by integration of (41) along a small neighbourhood of $t = 0$, it is found

$$[\![\dot{\epsilon}]\!] = 2\sqrt{h_0}\omega, \tag{42}$$

where $[\![f(0)]\!] = \lim_{t->0+} f(t) - \lim_{t->0-} f(t)$. Thus, it is concluded that the strain rate exhibits a jump in correspondence of $\varepsilon = 0$ and yet the dimensionless momentum as well as the kinetic energy are conserved

$$[\![p_0]\!] = \left[\!\left[\dot{\epsilon}^2\right]\!\right] = 0. \tag{43}$$

In particular, the last condition is possible only inasmuch as

$$\dot{\epsilon}(0^+) + \dot{\epsilon}(0^-) = 0, \tag{44}$$

which implies that simply the strain rate changes sign, as we already saw by looking at the phase diagrams. Conversely, moving in the neighbourhood of $p_0 \ll \varepsilon$, the first term in (34) disappears and we are left with the trajectories

$$\cos\theta = \frac{-\eta \pm \sqrt{h_0 + (\eta - 1)^2}}{1 + h_0 - 2\eta}.$$

Thus, the trivial solution is a saddle point that operates as an attractor.

3. Closed-form solution of the dynamics of the discrete system

Consider now the substitution $\varepsilon = \sec\theta - 1$ in the nonlinear ODE (8), whence we obtain the *linear* ODE

$$f(\theta, \dot{\theta}, \ddot{\theta}) = \omega^{-2}\ddot{\varepsilon} + \varepsilon - (\eta - 1), \tag{45}$$

whose solution can be immediately written as

$$\varepsilon(t) = c_1\cos(\omega t) + c_2\sin(\omega t) + \eta - 1. \tag{46}$$

Plugging this solution into the Hamiltonian (34), we find a connection between the constant c_1 and c_2 and the (conserved) energy of the system $h_0/2$, namely

$$c_1^2 + c_2^2 - (\eta - 1)^2 = h_0. \tag{47}$$

It is important to point out that the solution (46) is valid only inasmuch as the constraint (2) is satisfied. Let us assume that the boundary of this constraint is met at t_0 and define the solution $\varepsilon_0(t)$ in the time domain $t < t_0$ as

$$\varepsilon_0(t) = c_1\cos\left[\omega\left(t - t_0\right)\right] + c_2\sin\left[\omega\left(t - t_0\right)\right] + \eta - 1, \quad t < t_0, \tag{48}$$

and, obviously, the constraint $\varepsilon \geq 0$ is hit with speed

$$\dot{\epsilon}_0(t_0) = \omega c_2. \tag{49}$$

Beyond t_0, a new solution is defined

$$\varepsilon_1(t) = d_1\cos\left[\omega\left(t - t_0\right)\right] + d_2\sin\left[\omega\left(t - t_0\right)\right] + \eta - 1, \quad t > t_0, \tag{50}$$

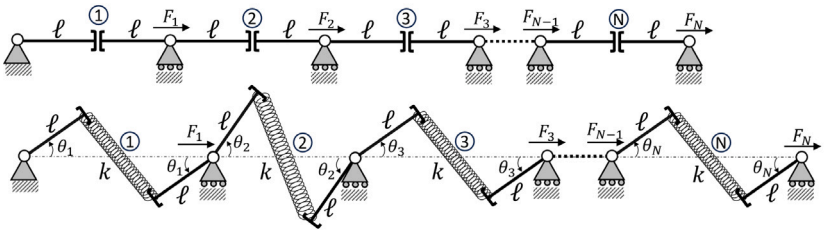

Fig. 10. N-term chain of bi-stable discrete mechanisms: trivial straight configuration (top) and buckled configuration (bottom) in the presence of the axial tension forces $F_i > F_{cr}$, $i = 1, \dots, N$.

where t_0 is a problem's unknown. The transfer conditions, connecting the constants c_1 and c_2 to the new constants d_1 and d_2 are given by

$$\varepsilon_0(t_0) = \varepsilon_1(t_0) = 0, \tag{51}$$

and by the strain rate jump (42). From the conditions (42) and (51), it is found

$$c_1 = d_1 = 1 - \eta, \quad d_2 = c_2 + 2\sqrt{h_0}, \tag{52}$$

and employing energy conservation (47) in Eq. (46) as well as in the corresponding expression involving the d_1 and d_2, one gets

$$c_2 = -\sqrt{h_0} = -d_2, \tag{53}$$

whence the strain rate flips sign across t_0, as already anticipated in the phase space analysis, and condition (44) is satisfied. It is concluded that the system behaves as a linear oscillator with respect to the strain ε, whose velocity (strain rate) bounces elastically upon hitting the constraint $\varepsilon \geq 0$, in much the same way as the simple pendulum would appear when considering the vertical strain coordinate as the dependent variable. Consequently, depending on what we agree to qualify as impact, we may say that no "real" impact occurs in this system, which conclusion may be supported by the fact that the momentum is indeed continuous across the impact time. In the next Section, we shall develop the continuous limit of this structure, in such a way that this energy conservation property is preserved.

4. Continuous limit of a dense chain of mechanisms

The near continuum limit of a spring–mass chain was first considered by Kruskal and Zabusky (1964) in connection with the Fermi-Pasta–Ulam (FPU) problem, and then revisited several times, for example by Rosenau (1986) and again lately in Rosenau (2003). The current literature focuses on spring–mass systems in the absence of unilateral constraints. Yet, the similarity of our dense chain to a spring–mass system is enough that we can still adopt a "continuation" procedure to obtain the system Lagrangian. Let us consider a finite sequence (chain) of discrete systems as in Fig. 10, numbered from 1 to N, which are merely interacting through the exchanged axial forces $\{F_n\}$. The *discrete* Lagrangian function of such a system reads

$$L_N = \sum_{n=1}^{N} \left(\tfrac{1}{2} m \dot{y}_n^2 - \tfrac{1}{2} F_{cr} 2\ell \tan^2 \theta_n + F_n y_n - F_{n-1} y_{n-1} \right), \tag{54}$$

where $y_n = y_n(t)$ is the longitudinal displacement of the right end of the nth discrete unit. To show that Eq. (54) specialized to a single system $n = N = 1$ indeed corresponds to (6), we use the connection

$$y_n = y_{n-1} + \varepsilon_{n-1}(2\ell), \tag{55}$$

whence, assuming the system is fixed at the left end, it is $y_0 = 0$ and (55) gives $y_1 = 2\varepsilon_0 \ell$ from which the kinetic energy becomes $K = \frac{1}{2} m (2\ell \dot{\varepsilon}_0)^2$ as in Eq. (5). Similarly, recalling the definition of strain (1), it is easily deduced that

$$\tan^2 \theta = (\varepsilon + 1)^2 - 1, \tag{56}$$

from which result the second term in the summation (54) is reduced to (the opposite of) the elastic potential energy, cf. Eq. (3), with the exception of the inessential constant contribution $-\frac{1}{2} F_{cr}$. Finally, the third term in (54) obviously lends the potential of the applied force, while the last term disappears in light of the boundary condition at the left end. It is emphasized that potential energy of this system is *convex* and, consequently, the *static* deformation of the continuum approximation is microscopically homogeneous, according to the Cauchy–Born rule, see Puglisi and Truskinovsky (2000). This means that the static investigation of a large number of units simply leads to the trivial result where all such units are equally deformed.

In the following, we shall adopt ε as the dependent variable and connect it to y through a Lagrange multiplier. A first important difference with the standard spring–mass chain theory lies in that the system is subjected to the unilateral constraint $\varepsilon \geq 0$, which

deeply affects its behaviour. In the limit as $N \to \infty$ and $\ell = \mathfrak{L}/N \to 0$ so that $\mathfrak{L} = N\ell$ and $F_{cr} = 2\ell k$ are finite and non-zero, we find the time density Lagrangian of the equivalent continuous system

$$L = \lim_{\substack{N\to\infty \\ \ell\to 0}} L_N - [\mathscr{F} y]_0^{2\mathfrak{L}}, \tag{57}$$

where and $\mathscr{F}(0)$ and $\mathscr{F}(2\mathfrak{L})$ are the prescribed loads at the system ends. With a bit of algebra, it is

$$L = \int_I \left[\tfrac{1}{2}\rho \dot{y}^2 - \tfrac{1}{2}F_{cr}(\varepsilon+1)^2 + F\varepsilon + F_{,x}y\right] \mathrm{d}x - [\mathscr{F} y]_{\partial I}, \tag{58}$$

where $I = [0, 2\mathfrak{L}]$ is the interval of integration and $\rho = (2\ell)^{-1}m$ is the mass density per unit length of the metastructure. In Eq. (58) it is assumed that $y_n(t) \to y(x,t)$ and $\varepsilon_n(t) \to \varepsilon(x,t)$ are independent functions, by virtue of the Lagrange multiplier $F_n(t) \to F(x,t)$ enforcing the constraint

$$\varepsilon = \partial y/\partial x = y_{,x}. \tag{59}$$

If Fy is assumed continuous along x, part integration yields

$$L = \int_I \left[\tfrac{1}{2}\rho \dot{y}^2 - \tfrac{1}{2}F_{cr}(\varepsilon+1)^2 + F(\varepsilon - y_{,x})\right] \mathrm{d}x + [(F-\mathscr{F})y]_0^{2\mathfrak{L}}, \tag{60}$$

Either Lagrangian (58) or (60) is the continuous limit of the discrete system (54) and corresponds to that of a tout string with tension F_{cr} and with constant pre-strain. Besides, the Lagrange multiplier F expresses the longitudinal force exchanged between adjacent discrete units, as in Fig. 10.

It is important to emphasize that the continuous system is also subjected to the *unilateral* (or not-holding) constraint

$$\varepsilon \geq 0, \tag{61}$$

which embodies the fact that each discrete unit may only elongate. In the language of convex analysis, we introduce the convex set of admissible elongations

$$\mathbf{K} = \{\varepsilon \in \mathscr{H}^1(I,T) : \varepsilon \geq 0 \text{ with boundary conditions}\}, \tag{62}$$

where $T = [t_0, t_1]$ is a time interval and we let the domain $\Omega = I \times T$. In the presence of an unilateral constraint, Hamilton's principle normally translates into the (elliptic) variational inequality (Rumyantsev, 2006)

$$\delta\mathscr{L} \leq 0, \tag{63}$$

where $\mathscr{L} = \int_T L\mathrm{d}t$ and equality holds for the so-called *loosened states*, for which the constraint is violated, i.e. $\varepsilon > 0$, and variations are reversible. The domain Λ, for which loosened states occur, is named the *noncoincidence set*

$$\Lambda = \{(x,t) \in \Omega : \varepsilon(x,t) > 0\}. \tag{64}$$

In contrast, the *coincidence set* is such that the constraint holds, i.e. these are constrained states

$$\Gamma = \{(x,t) \in \Omega : \varepsilon(x,t) = 0\}. \tag{65}$$

This variational problem may be recast in the form of a complementarity problem, through the *complementarity condition*

$$R\varepsilon = 0, \tag{66}$$

where, as we shall presently see, $R = F - N$ is the axial force in the rods in excess of the normal force $N = F_{cr}(\varepsilon+1)$. For discrete systems, the constraints and the complementarity condition

$$\varepsilon \geq 0, \quad -R \geq 0, \quad R\varepsilon = 0, \tag{67}$$

usually go under the name of Kuhn–Tucker conditions.

In the following, we shall show that this approach to the problem is unnecessary. Indeed, the appearance of the constraint (61) is only due to the choice of the dependent variables and not to the physics of the problem. In fact, we need to supplement a further condition on either continuous Lagrangian, so that it correctly portraits the constituent microstructure. As a result, the problem may be treated in standard fashion by a variational *equality*, although some care should be taken when dealing with discontinuities in the variables. Indeed, Appendix develops the procedure which allows to contemplate the presence of discontinuities in the variation process. Once this is accounted for, the standard Hamilton principle may be effectively used

$$\delta\mathscr{L} = 0, \tag{68}$$

with a great deal of simplification attached.

4.1. Hamilton's principle

The extra condition that needs to be imposed on either of the Lagrangians (58) or (60) is energy conservation, on account of the fact that, as we have already shown, each subunit of this system warrants that energy is preserved. Then, extending (Kozlov & Treshchëv, 1991)'s statement for discrete systems, "it turns out that Hamilton's principle is valid also for motions with impacts".

Taking variations of (58) as described in Appendix, we get the E-L equations (A.5) that read:

- the equilibrium equation

$$\rho\ddot{y} = F_{,x}, \tag{69}$$

- the constitutive equation $F = N$, where we have let the normal force in the chain

$$N = F_{cr}(\varepsilon + 1) \geq F_{cr}, \tag{70}$$

- the boundary conditions

$$[(\mathscr{F} - F)\delta y]_0^{2\mathfrak{L}} = 0. \tag{71}$$

Together, Eqs. (69), (70) and the constraint (59), that amounts to compatibility, lend d'Alembert wave equation

$$c_b^{-2}\ddot{y} - y_{,xx} = 0, \quad c_b = \sqrt{F_{cr}/\rho}, \tag{72}$$

whose general solution reads

$$y(x,t) = f(x - c_b t) + g(x + c_b t), \tag{73}$$

for any pair of functions $f(\xi)$ and $g(\xi)$, which are determined by the initial conditions. Similarly, from the natural boundary conditions (71), one gets, in view of (70),

$$[(\eta - \varepsilon - 1)\,\delta y]_0^{2\mathfrak{L}} = 0, \tag{74}$$

according to which it is either y fixed at the end points (regardless of F) or Eq. (36) holds, provided that $\eta \geq 1$ in light of the constraint. Interestingly, as in the discrete scenario, the emerging boundary value problem (BVP) is linear and it can be solved by variable separation

$$y(x,t) = e^{i\Omega t}\left[c_1 \sin\left(\frac{\Omega}{c_b}x\right) + c_2 \cos\left(\frac{\Omega}{c_b}x\right)\right]. \tag{75}$$

This solution is the continuum counterpart of (48) and we need to supplement the problem with time momentum π and energy H continuity across the time of impact, Eqs. (A.10), together with continuity of the reduced Lagrangian (A.11) at the impact location. The latter condition amounts to kinetic energy conservation and it is very important because it allows to continue the solution across the impact location thus building a sequence of solutions each of the form (75). We now look at energy conservation in more detail.

4.2. Hamiltonian of the continuous system

The Hamiltonian of the continuous system amounts to its energy

$$H = \int_0^{2\mathfrak{L}} h\mathrm{d}x, \quad h = \tfrac{1}{2}\rho^{-1}\pi^2 + \tfrac{1}{2}F_{cr}(\varepsilon + 1)^2 - F\varepsilon - F_{,x}y, \tag{76}$$

where $\pi = \rho\dot{y}$ is the time momentum conjugated with the velocity $\dot{y}$. To see this, we recall Eqs. (27), (34), from which we get

$$h = 2\ell F_{cr}\left[\frac{\dot{\varepsilon}^2}{2\omega^2} + \left(\tfrac{1}{2}\varepsilon^2 + \varepsilon\right) - \eta\varepsilon\right] = \tfrac{1}{2}(2\ell)^2\, m\dot{\varepsilon}^2 + 2\ell F_{cr}\left(\tfrac{1}{2}\varepsilon^2 + \varepsilon\right) - 2\ell F\varepsilon, \tag{77}$$

and summing over n discrete systems and in view of Eq. (55)

$$H_N = \sum_{n=1}^{2N}\left\{\tfrac{1}{2}m\left(\dot{y}_n - \dot{y}_{n-1}\right)^2 + 2\ell F_{cr}\left(\tfrac{1}{2}\varepsilon_n^2 + \varepsilon_n\right) - 2\ell F\varepsilon_n\right\}, \tag{78}$$

and finally taking the continuous limit

$$H = \int_0^{2\mathfrak{L}}\left[\tfrac{1}{2}\rho\dot{y}^2 + F_{cr}\left(\tfrac{1}{2}\varepsilon^2 + \varepsilon\right) - F\varepsilon\right]\mathrm{d}x. \tag{79}$$

Clearly, (79) corresponds to (76), apart from the inessential constant term $F_{cr}L$, provided that F is constant. Indeed, assuming that the constraint (59) is accounted for and that F is constant along x, the energy (76) is bounded from below, which property warrants that spurious short-wavelength instabilities, sometimes named ultra-violet, are absent, see Rosenau (2003).

Hamilton's canonical equations read

$$\frac{\partial h}{\partial \pi} = \rho^{-1}\pi = \dot{y}, \tag{80}$$

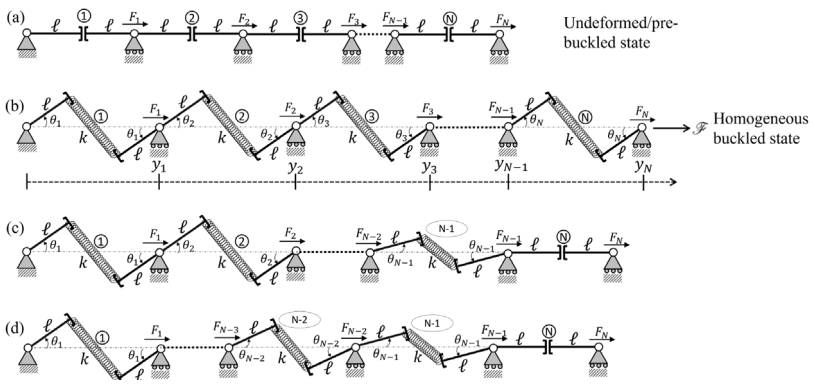

Fig. 11. Set-up of the semi-analytical solution: The continuous system is acted upon by a force $\mathscr{F} = F_{cr}\eta$, with $\eta = 1.1$, which causes it to buckle at all points (b), such force is then suddenly released at $t = 0$ (c) and longitudinal vibrations begin (d), with a wave moving towards the left end with speed c_b.

which is the definition of the time momentum, and

$$\frac{\partial h}{\partial y} = -F_{,x} = -\dot{\pi}, \tag{81}$$

that is the equilibrium equation (69). The variable ε is *kinostenic* or ignorable (Lanczos, 2012), and plain minimization lends the constitutive equation (70).

4.3. Semi-analytical solution of the continuous metastructure

We now solve the dynamics of the continuous system when the left end is fixed, the right end is subjected to a given force $\mathscr{F} = F_{cr}\eta$, with $\eta = 1.1$ (see Fig. 11). Therefore, in the initial stage $t < 0$, the strain is constant $\varepsilon(t, x) \equiv 0.1$ and the metastructure sits above the critical load at each point, in the buckled state, Fig. 11(b). The force is suddenly released at time $t = 0$ and from then longitudinal vibrations kick in, Fig. 11(c). To get rid of physical dimensions, we let $c_b = 1$ and $\mathfrak{L} = 1$, so that $x \in [-1, 1]$. In this scenario, a travelling elastic wave is triggered which, moving towards the fixed end, Fig. 11(d), determines a progressive reduction in ε which, eventually, hits the constraint (61) at time t_c and abscissa $x = x_c < 2\mathfrak{L}$, marking the transition from the supercritical to the subcritical regime.

Assuming that a single impact occurs, the solution (73) holds for $t < t_c$

$$y(x, t) = f_0(x - c_b t) + g_0(x + c_b t), \quad t < t_c, \tag{82}$$

and similarly for $t > t_c$

$$y(x, t) = \begin{cases} f_1(x - c_b t) + g_1(x + c_b t), & x < x_c, \\ f_2(x - c_b t) + g_2(x + c_b t), & x > x_c, \end{cases} \qquad t > t_c, \tag{83}$$

where $x_c = x_c(t), t \geq t_c$, is the impact location, that generally varies in time. Under the condition that displacement and tension are continuous in space across x_c, one gets two equations which relate f_1 and g_1 to f_2 and g_2, namely

$$f_1(\xi_c^-) + g_1(\xi_c^+) = f_2(\xi_c^-) + g_2(\xi_c^+), \quad f_1'(\xi_c^-) + g_1'(\xi_c^+) = f_2'(\xi_c^-) + g_2'(\xi_c^+), \tag{84}$$

where prime denotes differentiation with respect to the argument and $\xi_c^\pm = x_c \pm c_b t_c$. Likewise, continuity in time of the displacement and time momentum lends a pair of relations which connect f_0 and g_0 to f_1 and g_1 for $x < x_c$ and to f_2 and g_2 for $x > x_c$, say

$$\begin{aligned} &f_0(x - c_b t_c) + g_0(x + c_b t_c) = f_1(x - c_b t_c) + g_1(x + c_b t_c), \\ &-f_0'(x - c_b t_c) + g_0'(x + c_b t_c) = -f_1'(x - c_b t_c) + g_1'(x + c_b t_c), \end{aligned} \qquad x < x_c. \tag{85}$$

The set of Eqs. (84), (85) is generally sufficient to the full determination of $f_{1,2}$ and $g_{1,2}$ from f_0 and g_0, except at $x = x_c$ where the constraint is hit and therefore

$$f_0'(\xi_c^-) + g_0'(\xi_c^+) = f_1'(\xi_c^-) + g_1'(\xi_c^+) = f_2'(\xi_c^-) + g_2'(\xi_c^+) = 0, \tag{86}$$

which means that the solutions are no longer linearly independent. At this particular point in time and space we can no longer apply the second of (85) because a jump in the time momentum is expected, according to Eq. (A.12). Precisely this last condition is demanded to bridge in time across the impact and consequently integrate, in piecewise fashion, the dynamics of the system.

Fig. 12 plots the evolution in time of the incompressible system at selected time instants, from the release of the traction force ($t = 0$) until the elastic wave hits the left end ($t = 1200$). Around time $t = 400$, the axial incompressibility constraint is hit within the string (besides the right end where $\varepsilon \equiv 0$ on account of the absence of an applied tension). Fig. 12 should be compared with Fig.

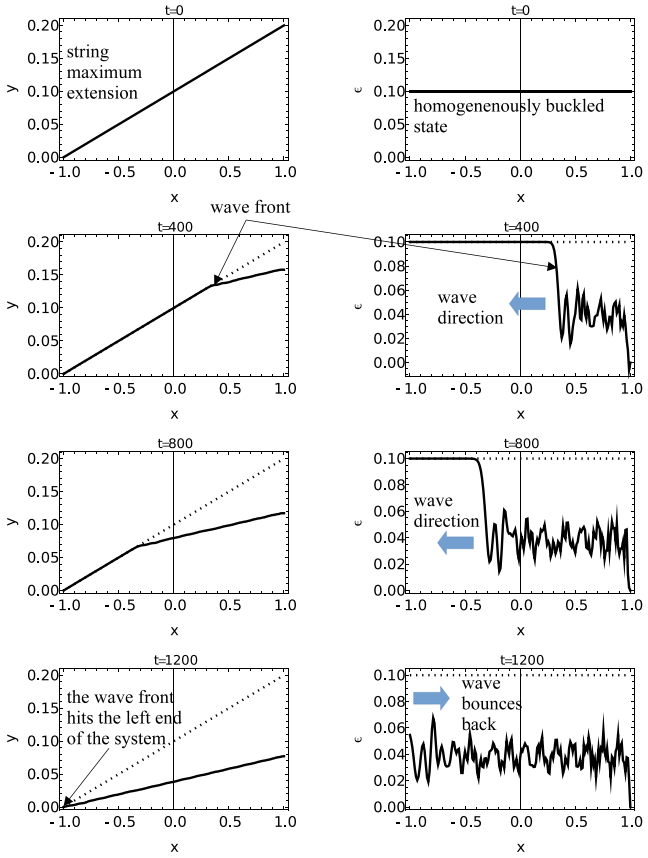

Fig. 12. Dimensionless longitudinal displacement y (left) and strain ϵ (right) vs. x at the dimensionless times $t = 0, 400, 800$ and 1200 for the incompressible string. This set of plots should be compared with Fig. 13 that shows the dynamics of the elastic string in the absence of the constraint (61).

13 that is obtained considering the classical elastic string, for which the constraint (61) is absent and d'Alembert's solution holds in the entire domain. For the sake of comparison and in an attempt to factor out numerical errors, the solution of the elastic string is obtained applying the same code used for the incompressible string by disabling the constraint check. In particular, it is seen that the incompressible string develops an almost constant positive strain *behind* the impact location, which progresses to the left with the speed c_b that is the same as for the classical string. Numerical oscillations appear as a consequence of the steep jump in the strain. The wave hits the fixed end $x = -1$ at a time near $t = 1200$ for both the incompressible and the compressible string. Finally, Fig. 14 shows that for both systems the energy is globally preserved, which is a consequence of the application of the variational condition (A.12).

5. Conclusions

In this paper we investigates the longitudinal dynamics of a continuous metastructure realized by a dense chain of bistable Single Degree of Freedom (SDOF) mechanisms which buckle under axial traction and are otherwise incompressible. To this aim, we first investigate the dynamics of the SDOF mechanism and observe that, under the viewpoint of the longitudinal deformation, it acts as an energy preserving unilateral constraint. Yet, we notice that the appearance of "impacts" in the system entirely disappears when the angular coordinate is adopted instead. Next, moving to the continuous limit of a dense chain of interconnected mechanisms, a continuous Lagrangian is obtained wherein the longitudinal strain naturally emerges as the dependent variable. With this, the related unilateral constraint also appears, this time over the continuum. Most importantly, we show that, to effectively portrait the dynamics of the underlying microstructure, the unilateral constraint embodying longitudinal incompressibility must be supplemented by the requirement that energy is preserved across the impacts. This feature has all-important consequences, above which the fact that the system may still be treated through a variational *equality* expressing Hamilton's principle, without the need to adopt the heavy machinery associated with variational inequalities and non-smooth mechanics. Of course, this is only possible provided that the variational procedure is extended to accommodate for jumps in the dependent variables, which provision introduces extra conditions, similar to the Weierstrass–Erdmann (W-E) conditions (Gelfand & Fomin, 1963), that define the transition through the impact location

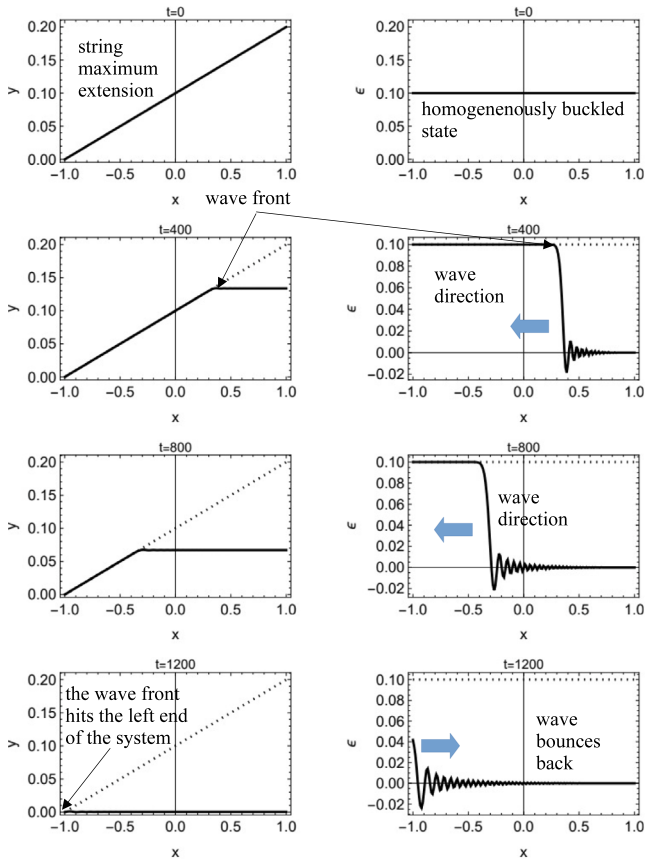

Fig. 13. Dimensionless longitudinal displacement y (left) and strain ϵ (right) vs. x at the dimensionless times $t = 0, 400, 800$ and 1200 for the elastic string, in the absence of the constraint (61). Without the constraint, negative strain values are admitted and behind the wave front the string is traction-free.

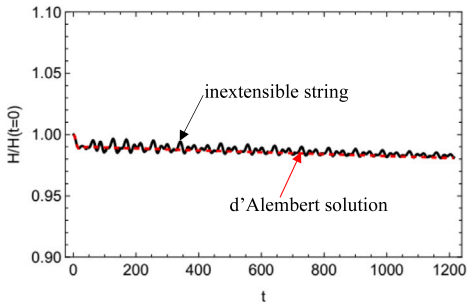

Fig. 14. Relative energy $H(t)/H(0)$ along time t for the system with (black, solid) and without (red, dashed) the constraint (61), as computed by the same code: Allowing for some numerical approximation connected to the quantized precision in the location of the impact (in time and space, which are discretized), the energy is globally preserved.

(in time and space). The governing equation of the system dynamics corresponds to that of an incompressible string. Through the extended W-E conditions, the semi-analytical solution of the system dynamics is obtained for the case when the system is statically extended by an end force that is then instantly removed. An elastic wave appears that moves from the now load-free end with the classical string wave speed. However, whenever the constraint is hit along the structure, multiple waves originate that move back towards the free end. To test the validity of the results, both systems are checked against global energy conservation in time.

CRediT authorship contribution statement

Andrea Nobili: Writing – review & editing, Writing – original draft, Visualization, Software, Investigation, Funding acquisition, Formal analysis, Conceptualization. **Dipendu Pramanik:** Visualization, Validation, Investigation.

Declaration of competing interest

The authors declare the following financial interests/personal relationships which may be considered as potential competing interests: Andrea Nobili reports financial support was provided by Italian government Ministry of University and Research (MUR). If there are other authors, they declare that they have no known competing financial interests or personal relationships that could have appeared to influence the work reported in this paper.

Acknowledgements

We acknowledge financial support under the National Recovery and Resilience Plan (NRRP), Italy, Mission 4, Component 2, Investment 1.1, Call for tender No. 1409 published on 14.9.2022 by the Italian Ministry of University and Research (MUR), funded by the European Union NextGenerationEU (NGEU), Project Title: Sustainable CompositE materials for the construction iNdusTry - CUP P2022P3Y2T - Grant Assignment Decree No. 1381 adopted on 1.9.2023 by the Italian Ministry of University and Research (MUR). This research was conducted under the auspices the National Group of Mathematical Physics (GNFM), a group of the Italian Institute of Higher Mathematics (INdAM).

Appendix. Extended for of the variation of the action that accounts for discontinuities

Following Kozlov and Treshchëv (1991), let us consider a family of continuous curves $y_\alpha(x,t), \varepsilon_\alpha(x,t)$ and $F_\alpha(x,t)$ where $x \in [a,b]$ and $t \in [t_1,t_2]$, while α is some parameter $\alpha \in (-\alpha_0,\alpha_0)$, so that the end values are fixed

$$y_\alpha(a,t) \equiv y_a(t), \quad y_\alpha(b,t) \equiv y_b(t), \quad F_\alpha(a,t) \equiv \mathscr{F}_a(t), \quad F_\alpha(b,t) \equiv \mathscr{F}_b(t). \tag{A.1}$$

Impact occurs in time at $t = t_\alpha$ and in space at $x = x_\alpha$ and, in general, it evolves along time: $x_\alpha = x_\alpha(t_\alpha)$. At impact, we have

$$F_\alpha(x_\alpha,t_\alpha) \equiv F_{cr}, \quad \varepsilon_\alpha(x_\alpha,t_\alpha) \equiv 0, \tag{A.2}$$

and we assume displacement continuity across time and space. In particular, for $\alpha = 0$, we get the extremal of Hamilton's problem with a non-smooth action, where $t_0 = t_c$ and $x_0 = x_c = x_c(t_c)$. Let us compute the variation of the action (58)

$$I_\alpha = \int_{t_1}^{t_2}\int_a^b L(y_\alpha,\dot{y}_\alpha,\varepsilon_\alpha,F_\alpha,F'_\alpha)\mathrm{d}x\mathrm{d}t, \tag{A.3}$$

where $\frac{\partial F_\alpha}{\partial x} = F'_\alpha$. For simplicity, let us first consider the single contribution

$$\hat{I}_\alpha = \int_{t_1}^{t_\alpha}\int_a^{x_\alpha} L(y_\alpha,\dot{y}_\alpha,\varepsilon_\alpha,F_\alpha,F'_\alpha)\mathrm{d}x\mathrm{d}t. \tag{A.4}$$

Thus, we get

$$\begin{aligned}\frac{\mathrm{d}\hat{I}_\alpha}{\mathrm{d}\alpha} &= \int_a^{x_\alpha}\left[\frac{\partial L}{\partial\dot{y}}\frac{\partial y_\alpha}{\partial\alpha}\right]_{t=t_1}^{t_\alpha}\mathrm{d}x + \int_{t_1}^{t_\alpha}\left[\frac{\partial L}{\partial F'}\frac{\partial F_\alpha}{\partial\alpha}\right]_{x=a}^{x_\alpha}\mathrm{d}t + \frac{\mathrm{d}t_\alpha}{\mathrm{d}\alpha}\int_a^{x_\alpha} L|_{t=t_\alpha}\mathrm{d}x \\ &+ \frac{\mathrm{d}x_\alpha}{\mathrm{d}\alpha}\int_{t_1}^{t_\alpha} L|_{x=x_\alpha}\mathrm{d}t + \int_{t_1}^{t_\alpha}\int_a^{x_\alpha}\left(-\frac{\partial}{\partial t}\frac{\partial L}{\partial\dot{y}} + \frac{\partial L}{\partial y}\right)\frac{\partial y_\alpha}{\partial\alpha}\mathrm{d}x\mathrm{d}t \\ &+ \int_{t_1}^{t_\alpha}\int_a^{x_\alpha}\left\{\frac{\partial L}{\partial\varepsilon}\frac{\partial\varepsilon_\alpha}{\partial\alpha} + \left(\frac{\partial L}{\partial F} - \frac{\partial}{\partial x}\frac{\partial L}{\partial F'}\right)\frac{\partial F_\alpha}{\partial\alpha}\right\}\mathrm{d}x\mathrm{d}t,\end{aligned}$$

that, accounting for the fact that the end points are fixed (A.1), becomes

$$\begin{aligned}\frac{\mathrm{d}\hat{I}_\alpha}{\mathrm{d}\alpha} &= \int_a^{x_\alpha}\left(\frac{\partial L}{\partial\dot{y}}\frac{\partial y_\alpha}{\partial\alpha} + L\frac{\mathrm{d}t_\alpha}{\mathrm{d}\alpha}\right)_{t=t_\alpha}\mathrm{d}x + \int_{t_1}^{t_\alpha}\left(\frac{\partial L}{\partial F'}\frac{\partial F_\alpha}{\partial\alpha} + L\frac{\mathrm{d}x_\alpha}{\mathrm{d}\alpha}\right)_{x=x_\alpha}\mathrm{d}t \\ &+ \int_{t_1}^{t_\alpha}\int_a^{x_\alpha}\left(-\frac{\partial}{\partial t}\frac{\partial L}{\partial\dot{y}} + \frac{\partial L}{\partial y}\right)\frac{\partial y_\alpha}{\partial\alpha}\mathrm{d}x\mathrm{d}t\end{aligned}$$

$$+\int_{t_1}^{t_\alpha}\int_{a}^{x_\alpha}\left\{\frac{\partial L}{\partial \varepsilon}\frac{\partial \varepsilon_\alpha}{\partial \alpha}+\left(\frac{\partial L}{\partial F}-\frac{\partial}{\partial x}\frac{\partial L}{\partial F'}\right)\frac{\partial F_\alpha}{\partial \alpha}\right\}\mathrm{d}x\mathrm{d}t.$$

In consideration of the fact that the families of curves y_α, ε_α and F_α are arbitrary inside the domain $(t_1,t_\alpha)\times(a,x_\alpha)$, we get the E-L equations

$$-\frac{\partial}{\partial t}\frac{\partial L}{\partial \dot{y}}+\frac{\partial L}{\partial y}=0, \tag{A.5a}$$

$$\frac{\partial L}{\partial \varepsilon}=0, \tag{A.5b}$$

$$\frac{\partial L}{\partial F}-\frac{\partial}{\partial x}\frac{\partial L}{\partial F'}=0, \tag{A.5c}$$

and we henceforth omit the last two integrals, under the assumption that the E-L equations are indeed satisfied. In view of the connections

$$\frac{\partial y_\alpha}{\partial \alpha}(x,t_\alpha)=\frac{\mathrm{d}}{\mathrm{d}\alpha}\left[y_\alpha(x,t_\alpha)\right]-\dot{y}_\alpha(x,t_\alpha)\frac{\mathrm{d}t_\alpha}{\mathrm{d}\alpha}, \tag{A.6}$$

$$\frac{\partial F_\alpha}{\partial \alpha}(x_\alpha,t)=\frac{\mathrm{d}}{\mathrm{d}\alpha}\left[F_\alpha(x_\alpha,t)\right]-\frac{\partial F_\alpha}{\partial x}(x_\alpha,t)\frac{\mathrm{d}x_\alpha}{\mathrm{d}\alpha}, \tag{A.7}$$

one gets

$$\frac{\mathrm{d}\hat{I}_\alpha}{\mathrm{d}\alpha}=\int_a^{x_\alpha}\left\{\frac{\partial L}{\partial \dot{y}}\frac{\mathrm{d}y_\alpha}{\mathrm{d}\alpha}+\left(-\frac{\partial L}{\partial \dot{y}}\dot{y}_\alpha+L\right)\frac{\mathrm{d}t_\alpha}{\mathrm{d}\alpha}\right\}_{t=t_\alpha}\mathrm{d}x$$
$$+\int_{t_1}^{t_\alpha}\left\{\frac{\partial L}{\partial F'}\frac{\mathrm{d}F_\alpha}{\mathrm{d}\alpha}+\left(-\frac{\partial L}{\partial F'}F'_\alpha+L\right)\frac{\mathrm{d}x_\alpha}{\mathrm{d}\alpha}\right\}_{x=x_\alpha}\mathrm{d}t.$$

Finally, one recognizes that L is a quadratic form in the velocity $\dot{y}$, whence

$$\frac{\partial L}{\partial \dot{y}}\dot{y}_\alpha=2K, \tag{A.8}$$

while L is a linear function of F', from which it is

$$-\frac{\partial L}{\partial F'}F'_\alpha+L=\tilde{L}(y,\dot{y},\varepsilon,F), \tag{A.9}$$

that no longer depends on F'. Thus, recalling that $H=K+V$ and accounting for the integral along $x\in(x_\alpha,b)$, it is

$$\frac{\mathrm{d}I_\alpha}{\mathrm{d}\alpha}=\int_a^b\left\{\frac{\partial L}{\partial \dot{y}}\frac{\mathrm{d}y_\alpha}{\mathrm{d}\alpha}-H\frac{\mathrm{d}t_\alpha}{\mathrm{d}\alpha}\right\}_{t=t_\alpha}\mathrm{d}x-\int_{t_1}^{t_\alpha}\left[\!\!\left[\frac{\partial L}{\partial F'}\frac{\mathrm{d}F_\alpha}{\mathrm{d}\alpha}+\tilde{L}\frac{\mathrm{d}x_\alpha}{\mathrm{d}\alpha}\right]\!\!\right]_{x=x_\alpha}\mathrm{d}t,$$

plus the E-L equations (A.5). If no impact occurs in the time interval (t_1,t_α), the second integral is zero. In general, however, we may take t_α arbitrarily, i.e. it may be any time when impact occurs, not necessarily the first time of impact, under the understanding that $t_0=t_c$ and the impact location follows accordingly: $x_0=x_c(t_c)$. Then, adding the contribution for $t\in(t_\alpha,t_2)$ and letting the axial momentum density and the energy of the system

$$\mathfrak{m}_\alpha(x,t)=\frac{\partial L}{\partial \dot{y}},\quad \mathscr{H}(t)=\int_a^b H\mathrm{d}x,$$

one writes

$$\frac{\mathrm{d}I_\alpha}{\mathrm{d}\alpha}=\int_a^b\left[\!\!\left[\mathfrak{m}_\alpha\frac{\mathrm{d}y_\alpha}{\mathrm{d}\alpha}\right]\!\!\right]_{t=t_\alpha}\mathrm{d}x-[\![\mathscr{H}]\!]_{t=t_\alpha}\frac{\mathrm{d}t_\alpha}{\mathrm{d}\alpha}-\int_{t_\alpha}^{t_2}\left[\!\!\left[\tilde{L}\frac{\mathrm{d}x_\alpha}{\mathrm{d}\alpha}\right]\!\!\right]_{x=x_\alpha}\mathrm{d}t,$$

because $\mathrm{d}F_\alpha/\mathrm{d}\alpha(x_\alpha(t),t)=0$ in light of the first of (A.2). For arbitrary variations of the displacement at the time of the impact, $y_\alpha(x,t_\alpha)$, and of the impact time itself, t_α, we get the continuity of momentum density and of the system hamiltonian across time

$$[\![\mathfrak{m}]\!]_{t=t_\alpha}=0\quad [\![\mathscr{H}]\!]_{t=t_\alpha}=0, \tag{A.10}$$

except at the impact location. By arbitrary variations of the impact location x_α at any given time, we also obtain continuity of the reduced Lagrangian

$$\left[\!\!\left[\tilde{L}\right]\!\!\right]_{x=x_\alpha}=0, \tag{A.11}$$

which, in view of Eqs. (A.2), yields continuity of the kinetic energy

$$\left[\!\!\left[\dot{y}^2\right]\!\!\right]_{x=x_\alpha}=0. \tag{A.12}$$

Data availability

No data was used for the research described in the article.

References

Brogliato, B. (1999). Nonsmooth mechanics. *vol. 3*, Springer.

Coulais, C., Teomy, E., de Reus, K., Shokef, Y., & van Hecke, M. (2016). Combinatorial design of textured mechanical metamaterials. *Nature*, *535*(7613), 529–532.

Florijn, B., Coulais, C., & van Hecke, M. (2014). Programmable mechanical metamaterials. *Physical Review Letters*, *113*(17), Article 175503.

Gelfand, I., & Fomin, S. (1963). Calculus of variations. Prentice-Hall Inc., NY, USA, Revised English edition translated and edited by Richard A. Silverman.

Gladman, A. S., Matsumoto, E. A., Nuzzo, R. G., Mahadevan, L., & Lewis, J. A. (2016). Biomimetic 4D printing. *Nature Materials*, *15*(4), 413–418.

Hima, N., Bigoni, D., & Dal Corso, F. (2022). Buckling versus unilateral constraint for a multistable metamaterial element. *Philosophical Transactions of the Royal Society, Series A*, *380*(2231), Article 20220021.

Hima, N., D'Annibale, F., & Dal Corso, F. (2023). Non-smooth dynamics of buckling based metainterfaces: rocking-like motion and bifurcations. *International Journal of Mechanical Sciences*, *242*, Article 108005.

Holmes, D. P., Roché, M., Sinha, T. K., Jung, S., & Stone, H. A. (2010). Bending and twisting of soft materials. *Soft Matter*, *6*(18), 4287–4292.

Hutchinson, J. W. (1974). Plastic buckling. *Advances in Applied Mechanics*, *14*, 67–144.

Kozlov, V., & Treshchëv, D. (1991). Billiards: A genetic introduction to the dynamics of systems with impacts. *vol. 89*, American Mathematical Soc..

Kravchuk, A. S., & Neittaanmäki, P. J. (2007). Variational and quasi-variational inequalities in mechanics. Springer.

Kruskal, M. D., & Zabusky, N. J. (1964). Stroboscopic-perturbation procedure for treating a class of nonlinear wave equations. *Journal of Mathematical Physics*, *5*(2), 231–244.

Lanczos, C. (2012). The variational principles of mechanics. Courier Corporation.

Lee, C.-M., & Goverdovskiy, V. (2012). A multi-stage high-speed railroad vibration isolation system with negative stiffness. *Journal of Sound and Vibration*, *331*(4), 914–921.

Mukhopadhyay, T., Ma, J., Feng, H., Hou, D., Gattas, J. M., Chen, Y., & You, Z. (2020). Programmable stiffness and shape modulation in origami materials: Emergence of a distant actuation feature. *Applied Materials Today*, *19*, Article 100537.

Overvelde, J. T., Shan, S., Bertoldi, K., et al. (2012). Compaction through buckling in 2D periodic, soft and porous structures: effect of pore shape. *Advanced Materials*, *24*(17), 2337–2342.

Palumbo, S., Deseri, L., Owen, D. R., & Fraldi, M. (2018). Disarrangements and instabilities in augmented one-dimensional hyperelasticity. *Proceedings of the Royal Society A: Mathematical, Physical and Engineering Sciences*, *474*(2218), Article 20180312.

Pocivavsek, L., Dellsy, R., Kern, A., Johnson, S., Lin, B., Lee, K. Y. C., & Cerda, E. (2008). Stress and fold localization in thin elastic membranes. *Science*, *320*(5878), 912–916.

Puglisi, G., & Truskinovsky, L. (2000). Mechanics of a discrete chain with bi-stable elements. *Journal of the Mechanics and Physics of Solids*, *48*(1), 1–27.

Rafsanjani, A., & Bertoldi, K. (2017). Buckling-induced kirigami. *Physical Review Letters*, *118*(8), Article 084301.

Rafsanjani, A., Zhang, Y., Liu, B., Rubinstein, S. M., & Bertoldi, K. (2019). Morphable concave–convex patterns in elastomers with embedded distributed bistable elements. *Advanced Materials*, *31*(6), Article 1804215.

Rosenau, P. (1986). Dynamics of nonlinear mass-spring chains near the continuum limit. *Physics Letters. A*, *118*(5), 222–227.

Rosenau, P. (2003). Hamiltonian dynamics of dense chains and lattices: or how to correct the continuum. *Physics Letters. A*, *311*(1), 39–52.

Rumyantsev, V. (2006). Variational principles for systems with unilateral constraints. *Journal of Applied Mathematics and Mechanics*, *70*(6), 808–818.

Shan, S., Kang, S. H., Raney, J. R., Wang, P., Fang, L., Candido, F., Lewis, J. A., & Bertoldi, K. (2015). Multistable architected materials for trapping elastic strain energy. *Advanced Materials*, *27*(29), 4296–4301.

Volpini, V., Giubilini, A., Corsi, L., Nobili, A., & Bondioli, F. (2022). Characterization of biocompatible scaffolds manufactured by fused filament fabrication of poly (3-hydroxybutyrate-co-3-hydroxyhexanoate). *Royal Society Open Science*, *9*(4), Article 211485.

Waitukaitis, S., Menaut, R., Chen, B. G.-g., & Van Hecke, M. (2015). Origami multistability: From single vertices to metasheets. *Physical Review Letters*, *114*(5), Article 055503.

Yap, H., Lakes, R., & Carpick, R. W. (2008). Negative stiffness and enhanced damping of individual multiwalled carbon nanotubes. *Physical Review B - Condensed Matter and Materials Physics*, *77*(4), Article 045423.

Zaccaria, D., Bigoni, D., Noselli, G., & Misseroni, D. (2011). Structures buckling under tensile dead load. *Proceedings of the Royal Society A: Mathematical, Physical and Engineering Sciences*, *467*(2130), 1686–1700.